UPPSALA
UNIVERSITET

UPTEC K 22010
Examensarbete 30 hp
Juni 2022

Drug Design of β-Lactamase Inhibitors of the DBO-scaffold against OXA-48

A Molecular Dynamics Study of Ligand Stability in the Michaelis Complex

Linda Liljeholm

Civilingenjörsprogrammet i kemiteknik

UPPSALA UNIVERSITET

Drug Design of β-Lactamase Inhibitors of the DBO-scaffold against OXA-48

Linda Liljeholm

Abstract

The emergence of β-lactamase-mediated antibiotic resistance is one of the biggest threats in modern times. Combined with the discovery void of new forms of antibiotics, this sets the course toward a future where the efficacy of present-day health care will be jeopardized. To hinder the spread of β-lactamase-mediated antibiotic resistance, the development of the drug class β-lactamase inhibitors has been prioritized. The foremost candidate for development of this drug class, that has wide-spectrum inhibition of β-lactamases, is the clinically available avibactam of the diazabicyclooctane-scaffold (i.e., DBO-scaffold). However, the clinical applications of this inhibitor have been limited against one of the more rapidly spreading β-lactamases; OXA-48. In order to bolster the drug development of β-lactamase inhibitors of the DBO-scaffold, with good inhibitory activity toward OXA-48, DBO-ligands with different structure elements were analyzed for stability of the Michaelis Complex in the OXA-48 binding site using molecular dynamic simulations. The results indicate that elongation of the chain to the anionic group of the ligand combined with the addition of a methyl group to the DBO-ring was stabilizing for the productive position between the backbone hydrogens of Y211 and S70. The binding affinity was also estimated using the Linear Interaction Energy method, and an offset parameter of $\gamma \approx -19$ kcal/mol was found and could represent the entropic differences of a flexible ligand-protein system. The results of this study may also indicate that the ligand stability of the Michaelis Complex is of minor consequence to the inhibition mechanism as a whole compared to the reaction rate.

Teknisk-naturvetenskapliga fakulteten

Uppsala universitet, Utgivningsort Uppsala

Handledare: Yasmin Binti Shamsudin Ämnesgranskare: Henning Henschel

Examinator: Christian Sköld

Populärvetenskaplig sammanfattning

Hotet om antibiotikaresistens på horisonten är ett välkänt fenomen, men exakt hur brådskande hotet är har underskattats då spridningen av problemet har stadigt ökat över en väldigt lång tid. Alexander Fleming, nobelpristagare för upptäckten av penicillinet, varnade vid sin Nobelföreläsning år 1945 att det är enkelt för bakterier att bilda resistens genom att utsätta dem för otillräckliga doser av antibiotika. Bakterier har nämligen gjort evolutionär utveckling för överlevnad till en konstform där allt som krävs för att resistens ska spridas är att *en* bakterie överlever dosen av antibiotika. Denna evolutionära fördel, kombinerat med överanvändningen och feldoseringen av antibiotika på en samhällsnivå, har lett till att resistensen fortsatt exponentiellt ökar med tid.

Modern sjukvård är starkt beroende av att antibiotika bevarar sin effekt för att t.ex. behandla cancerpatienter med nedsatt immunförsvar, behandla förtidigt födda barn samt för att utföra avancerade kirurgiska ingrepp. Fortsätter utvecklingen av denna resistens så väntar en dystopisk framtid där även relativt minimala infektioner kan bli minst lika angelägna som ovannämnda ingrepp. Dessvärre finns redan idag exempel på bakterier som genetiskt framställt enzymer som kan bryta ned även de senaste antibiotikasorterna. Ett av dessa ämnen har benämnts OXA-48, en så kallad β-laktamas, som har varit fokuset i detta arbete.

För att bromsa framfarten av bakterieframställda enzym som OXA-48 har en läkemedelsgrupp vid namn β-laktamashämmare utvecklats. β-laktamashämmare har som funktion att rädda antibiotikan från att brytas ned av dessa enzym, vilket har chansen att öka livslängden och återge effekten av antibiotika hos redan resistenta bakterier. Del av problematiken att utveckla läkemedel mot OXA-48 är att de flesta varianter av kliniskt använda β-laktamashämmare har minimal effekt. Den β-laktamashämmare som just nu har bäst effekt och även bäst potential för vidareutveckling är läkemedlet avibactam, vilket har en specifik grundstruktur som kallas diazabicyklooktan (DBO)-strukturen. I detta arbete så har avibactam och liknande molekyler av DBO-strukturen undersökts för att utforska åt vilket håll vidareutvecklingen av dessa β-laktamashämmare behöver gå för att stärka effekten mot OXA-48.

Ändlöst många variationer av DBO-strukturen kan vara möjliga, där även en liten förändring kan ha stor betydelse för effekten av läkemedlet. Tusentals molekyler kan syntetiseras för att beprövas experimentellt, men risken är stor att majoriteten av dessa molekyler inte har duglig verkan. Detta beror på komplexiteten hos OXA-48 och bristen på kunskap om hur detta enzym fungerar. Istället för att endast förlita sig på experimentella prövningar så kan man använda sig av databaserade modelleringsmetoder. Genom dessa metoder kan man få insikt hur en läkemedelskandidat av DBO-strukturen skulle interagera med OXA-48, hur olika variationer i läkemedlets struktur skulle leda till förbättring eller försämring och vidare bidra till kunskapen om funktionen av OXA-48.

För att främja användningen av databaserade modelleringsmetoder, som fortsatt kommer ha en viktig roll i läkemedelsindustrin, användes dessa metoder för att utvärdera avibactam och för att göra jämförelser med andra variationer av β-laktamashämmare med DBO-strukturen mot OXA-48. Resultaten visade på vilka interaktioner med OXA-48 som var viktiga för stabiliteten av läkemedel med DBO-strukturen, hur olika strukturelement kan gynna dessa interaktioner samt hur framtidens avibactam skulle kunna se ut. Utifrån dessa databaserade modelleringsmetoder har även beräkningsmetoder för att kvantitativt bestämma kompatibiliteten mellan läkemedlet och OXA-48 använts. Detta arbete kan bidra till pusselbitar som behövs för en bättre förståelse av β-laktamashämmares design mot OXA-48, med det långsiktiga målet att bevara antibiotikans verkan för att behålla vigilansen mot bakterieinfektioner.

Table of Contents

Introduction

Bacterial antimicrobial resistance, or as it is more commonly referred to in everyday speech: antibiotic resistance, has become one of the most pressing public health threats of the 21st century. According to a publication released in January of 2022, an estimated 4.95 million deaths associated with antibiotic resistance were reported in 2019 whereas 1.27 million deaths could be directly attributed to it [1]. If left unchecked, the situation will become even more lethal in the future due to the persistence and spread of multi-drug resistant bacteria or "superbugs", where a minor wound could end up being fatal.

Antibiotic resistance is conferred via the development of protective mechanisms in microorganisms, an evolutionary tendency partly caused by overexposure to antibiotics due to excessive use and insufficient dosing [2]. There are multiple ways in which a microorganism may protect itself, but one of the more common ones entails enzymatic degradation of the antibiotic. Among these enzymes are the β-lactamases, which is named after their degradation mechanism of the four-membered β-lactam ring part of the structure of antibiotics.

β-lactamases are proteins that come in wide structural variety and are separated into classes based on the conserved and distinguishing amino acid motifs – class A, B, C, and D β-lactamases [3]. Despite a few differing residues in the active site, the enzymatic activity is similar for classes A, C, and D; these are called the serine β-lactamases as the serine residue is the key component of the degradation of the substrate. Class B β-lactamases are called metallo-β-lactamases as the degradation of the substrate is facilitated via a zinc ion in the active site.

Within these classes, there are families and sub-families of enzymes. Class D has the least number of families (14 in contrast to the 104 families in class A), where the OXA-family stands for the vast majority of the members [4]. OXA, short for oxacillinase, received its abbreviated name from showing enhanced activity against the semi-synthetic penicillin called oxacillin. The OXA-family originally received little attention as these β-lactamases were relatively rare and with a narrow substrate profile, compared to the ubiquitous class A TEM-enzymes [5]. It was not until the explosive global emergence of OXA family members in the 1980s and onwards, that most of them were carbapenem-hydrolyzing class D β-lactamases (or carbapenemases), that the OXA-β-lactamases began to pose a clinically major problem.

Carbapenems are considered the last-resort antibiotics, and since the release of the carbapenem in 1985, there has been a discovery void of any new antibiotics [6]. The emergence of multiple new carbapenemases is an urgent global threat. While multiple OXA sub-families are carbapenemases, the most clinically relevant ones are OXA-23-, OXA-24/40-, and OXA-48-like β-lactamases [4]. OXA-48-like β-lactamases are especially urgent as, unlike its other sub-families, they are dispersed among *Enterobacteriaceae*, where infections caused by this group of Gram-negative bacteria are truly pathogenic and able to infect immunocompetent individuals [7].

Hence, carbapenem efficacy needs to be preserved to sustain resilience against Gram-negative bacterial infections. One strategy is the development of β-lactamase inhibitors that will save the antibiotic from degradation by blocking the active site of the enzyme. However, this has proved to be challenging against the OXA-family. Commercially available inhibitors, such as β-lactam-derived clavulanic acid, tazobactam, and sulbactam, that are active against other classes of β-lactamases do not inhibit class D β-lactamases [8].

Building upon scaffolds different from the β-lactam-derived inhibitors has been prioritized in finding new inhibitor leads, where many variants are undergoing clinical trials – either as a

standalone inhibitor or by synergistic activity with an antibiotic [9]. Non-β-lactam inhibitor scaffolds include diazabicyclooctane-derived (DBO, e.g., avibactam) as well as the recent boronic acid-derived inhibitors (e.g., vaborbactam). The DBO avibactam currently poses the greatest potential, as it is the primary non-β-lactam-derived β-lactamase inhibitors in use today. In 2015 the combination of the antibiotic ceftazidime and avibactam was approved for clinical use, where avibactam was able to redeem efficacy to treat ceftazidime-resistant bacteria [10,11]. Avibactam has shown to be an excellent inhibitor to class A and C enzymes, and while an improvement, the inhibitory effect still varies toward most class D enzymes [12].

The wide diversity of OXA-enzymes has stumped the development of effective inhibitors, while there is also a gap in knowledge about the molecular details of the inhibition mechanism itself. Derivatives of avibactam built upon the DBO-scaffold have since been synthesized in a wide variety, where *in vitro* assays have shown both hits and misses in terms of the inhibitory ability for OXA-48 [13,14]. An alternative route to drug development not yet employed in the search for a new β-lactamase inhibitor is virtual screening, which is a computer-based method that simulates the drug molecule in the protein target. Virtual screening methods applied for structure-based design are more cost-effective than high-throughput screening methods and not too time-consuming even without heavy-duty computational power. As the performance of computers is constantly improving, *in silico* methods have become more and more integrated into the drug development process. Virtual screening has already been successfully applied in the development of drugs such as captopril (antihypertensive drug), saquinavir, ritonavir, and indinavir (HIV treatment) among others [15].

This project aims to apply structure-based design methods using molecular dynamics (MD) simulations to identify structure elements of β-lactamase inhibitors with the DBO-scaffold and important protein interactions to improve the stability in the Michaelis Complex during the preliminary stage of the inhibition mechanism of OXA-48. The ligands to be investigated are the clinically used avibactam and its derivative relebactam, as well as the investigational drugs from Durand-Réville et. al. referred to in this project as ETX and ETX-F (figure 1) [14]. The binding affinity will also be estimated by calculating the free binding energies using the Linear Interaction Energy (LIE) method and compared with experimentally determined binding affinities from IC_{50}-values (see figure 1). The general workflow has been applied in a study by Shamsudin et. al. for the ligand design of COX-1 inhibitors [16] but has not yet been used for β-lactamase inhibitor design and could bolster the drug design of future β-lactamase inhibitors.

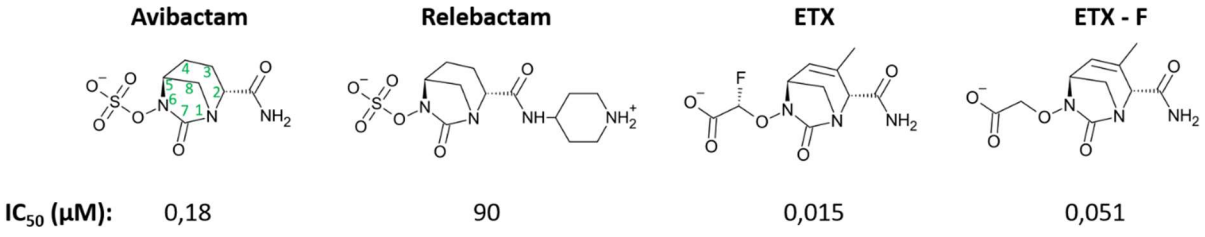

Figure 1: Structures, the numbering of the DBO-ring, and charges of each ligand at pH 7.0. The IC_{50}-values for each ligand are reported in µM. The IC_{50}-values for avibactam and relebactam were determined at 310 K [17], while the IC_{50}-values for ETX were determined at 298 K [14].

Background

Structure of OXA-48

In the structure of OXA-48, three motifs that are broadly conserved within class D enzymes are present [18]. Motif I include the catalytically important S70 and K73 of the binding site, motifs II and III are in the vicinity of these key residues (figure 2). Motif II includes residues S118-

V119-V120 and resides at the α4-α5 loop (green). Motif III includes K208-T209-G210-Y211, where K208 and T209 together with R250 make up a basic patch deeper into the binding site (dark blue). Beyond these conserved motifs, the Ω-loop (yellow; residues 143-165) together with the β5-β6 loop (cyan; residues 213-218) are catalytically important for the OXA-48 enzyme, as they provide electrostatic stability to the binding site [2]. The long and flexible α3-α4 loop has also been shown to be important for OXA-48 enzymes in widening the binding site to allow the opening of a water channel part of the hydrolysis of antibiotics [19].

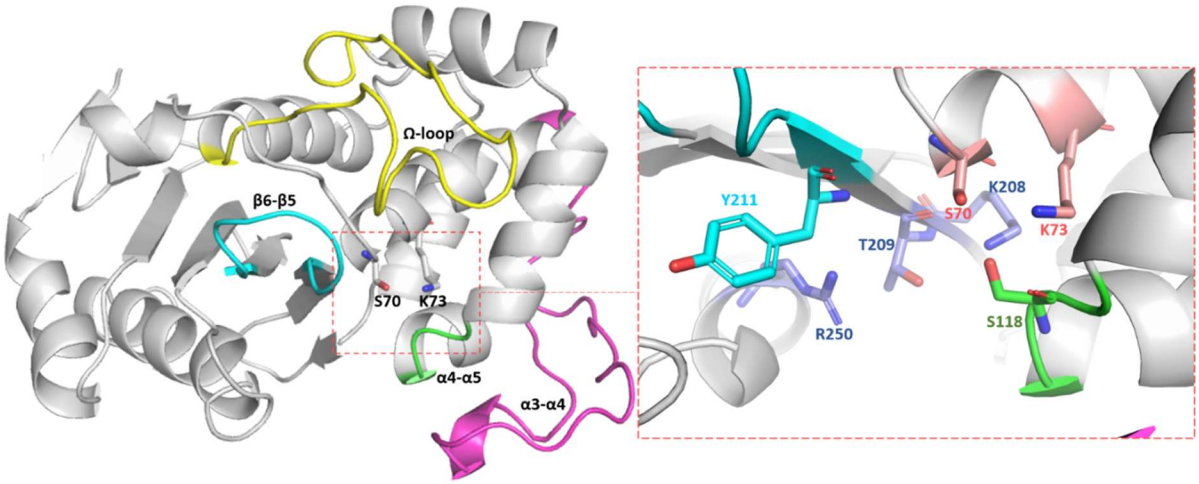

Figure 2: Full structure of the OXA-48 monomer with highlighted chains of interest (left) and an enhanced depiciton of the binding site with highlighted residues (right).

Mechanism of Inhibition with Avibactam

The basic patch consisting of R250, T209, and K208 part of motif III anchors the substrate in the binding site by a salt-bridge interaction mainly between R250 and the anionic functional group of the substrate. The initiation of the mechanism is via the activation of S70 (figure 3), which is activated via deprotonation from K73 acting as a general base. The course of events for how K73 activates S70 has two possible routes (based on what is currently known); either K73 is carboxylated (from a reaction with dissolved CO_2) and carries a negative charge that deprotonates S70, or the residue is momentarily neutral and the free electron pair of the nitrogen deprotonates S70. While the carboxylation of K73 appears to have importance in the mechanism for degrading antibiotics [20], it may not actively participate in the inhibition mechanism – specifically in the activation of S70. Studies suggest that the carboxylation of K73 is reversible and its occurrence is favored by a higher pH (pH ~8), but in the presence of covalently binding inhibitors, such as avibactam at physiological pH, the residue is carboxylated to a lesser degree [2,21]. K73 is not likely to exist as neutral in a physiological environment, but as the carboxylation reverses when the Michaelis Complex ensues there may be a window where K73 is briefly neutral – this hypothesis is the basis for the state used for the molecular dynamic simulations in this project.

The activated S70 will perform a nucleophilic attack on the carbonyl carbon in the DBO ring of avibactam, forming a tetrahedral intermediate stabilized by the oxyanion hole which is made up of the backbone of residues Y211 and S70. The lone electron pair on the oxygen will drive back the carbonyl formation, which in turn will break up the ring of avibactam by the nitrogen to the sulfate group, creating a carbamyl-enzyme complex. Avibactam is a reversible inhibitor, and while the binding into the enzyme is fast, the recyclization and subsequent decarbamylation of the structure is a relatively slow process.

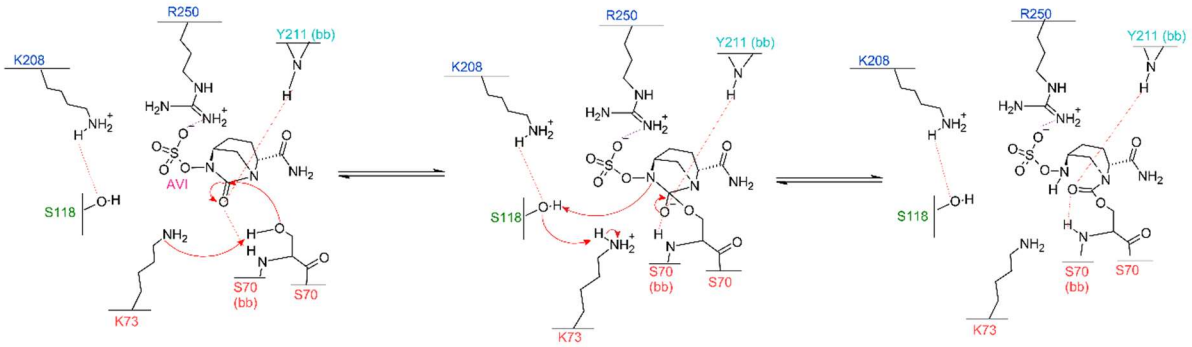

Figure 3: Inhibition mechanism of Avibactam derived from the study by King et. al. [2]. (bb): backbone; dashed lines indicate backbone-interactions with the carbonyl oxygen.

Experimental – Computational Method

The general workflow for this project is depicted in figure 4. The method is divided into four main steps; the preparation step (yellow), the molecular docking step (green), the MD simulation step with a focus on system stability (blue), and the final step of MD simulations with a focus on binding free energy determination (red). The MD simulation steps are repeating processes, where the model system is constantly evaluated and re-run until stability is achieved.

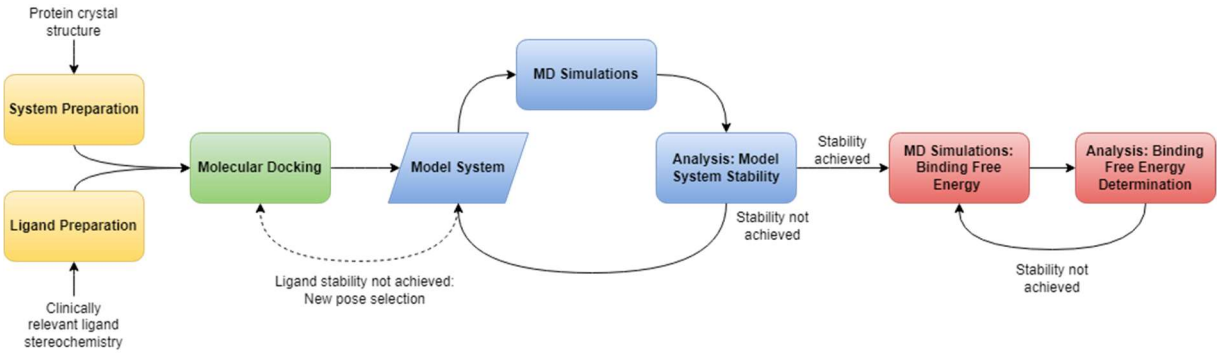

Figure 4: General workflow of the method used in the project. The abbreviation MD stands for "Molecular Dynamics".

System and Ligand Preparation

The protein system was prepared from the crystal structure of OXA-48 in complex with avibactam (PDB ID: 4S2K), captured with X-ray diffraction at a resolution of 2.10 Å. Stabilizing ions, co-crystallized water molecules, and the covalently bound avibactam were all removed from the structure using the Protein Preparation Wizard function [22] in Maestro (ver. 13.0) [23] from the Schrödinger Suite (ver. 2021-4). OXA-48 was captured in the crystal structure as a homo-dimer, i.e., consisting of two identical protein chains, so for computational simplicity, the system was reduced in size by only preparing chain A. Again, using the Protein Preparation Wizard function, the protein was pre-processed by adding missing hydrogens, creating disulfide bonds and generating charged residues at pH 7.0. The system was then refined by optimizing the hydrogen bond assignment and the structure underwent restrained minimization by applying the force field OPLS4 [24].

The ligands used during this project were generated using the 2D Sketcher in Maestro with clinically relevant stereochemistry. Using the LigPrep-function [25], the ligands were ionized at pH 7.0 and minimized with OPLS4.

Molecular Docking

The prepared ligands were docked into the prepared protein system using the docking program GLIDE ("Grid-based Ligand Docking with Energetics", ver. 9.3) [26] from the Schrödinger Suite. A docking grid was first generated using the Receptor Grid Generator to constrain the docking site of the ligand. The enclosing box of the grid had a size of 10 Å and the center point was supplied from the coordinates of the β-carbon in the residue S70.

When generating ligand poses from the docking, GLIDE has two scoring functions that were used when screening for the appropriate pose – Standard Precision (SP) and Extra Precision (XP). These scoring functions approximate the binding energies following physical chemistry principles (hydrogen bonding, lipophilic interactions, solvent exposure, etc.) and generate output-poses listed from highest to lowest score, but the weights of the various terms for each scoring function are different. The difference between the scoring functions is the penalties applied to the score of a pose from any violations, where XP applies harsher penalties to poses where charged or highly polar groups are desolvated. SP thus allows for more flexibility of the ligand placements within the docking site, whereas XP is less flexible in exchange for a higher probability of eliminating false positives in the output poses.

The ligand pose output was set to a maximum of 10 for either scoring function, where the generated poses of the ligand were evaluated per the proximity of the DBO-carbonyl to S70, stabilizing interactions to protein residues (primarily hydrogen bonds and salt bridges) and the overall GlideScore. A primary pose is selected from this evaluation and is screened for stability in the following step.

Molecular Dynamics – Model System Stability

The selected primary pose generated from the ligand docking was then simulated using the molecular dynamics program Desmond [27] provided in the Schrödinger Suite. The system was prepared using the System Builder, where the system with the docked ligand was solvated using the TIP3P model [28] (water solvated) in an orthorhombic box shape with a buffer distance of 10 x 10 x 10 $Å^3$, and minimized using OPLS4. The system was neutralized by supplementing ions calculated according to the net charge of the full system. The simulation file was created using the Molecular Dynamics function where, except for the simulation time and temperature, the Desmond default were set for the parameters. For the simulation time, 10 ns was initially used to screen the selected ligand pose where, if it seemed stable, it was subsequently simulated for 50 ns to evaluate the long-term behavior in the binding site. The temperature for the simulations depends on the temperature used when determining the IC_{50}-values of each ligand, where avibactam and relebactam were simulated in 310 K while ETX and ETX-F were simulated in 298 K.

The simulations were run in five replicates per pose with randomized initial velocities. The stability of the system was determined by plotting the Protein-Ligand Root Mean Square Deviation (PL-RMSD), which is a function that is part of the Simulation Interaction Diagram function of the Schrödinger Suite. The PL-RMSD is a measure of the average change in displacement of the system throughout the simulation, which can indicate if the protein has equilibrated or if bigger conformational changes have occurred. Similarly, the stability of the ligand in relation to the protein can be seen, where fluctuations could indicate diffusion from the initial docking position. If stability of the ligand for the selected primary pose was not achieved, a new pose was selected from the output poses generated in the molecular docking step.

The distance between the carbonyl of the DBO-ring in the ligands and catalytically important residue S70 was also measured throughout the 50 ns simulations to find the distribution of ligand positions within the binding site.

Molecular Dynamics – Binding Free Energy Determination with LIE

By using the molecular dynamics program Q (ver. 5.06) [29], the free binding energies can be calculated in biomolecular systems, solvated in a sphere of water molecules. Q bases the simulations on the spherical boundary condition (SBC) model, where the system is divided into three subshells: the outermost (frozen) layer representing bulk water, the middle layer which surrounds the innermost layer containing the main point of interest for molecular dynamic simulation, which in this system contains the binding site and ligand. The middle and innermost layers are where the system is unconstrained, which allows for solutes and solvents to move freely to simulate a real biological system. The boundary between the outermost and middle layer employs a half-harmonic potential that keeps the solvent from moving outside the boundary, which sustains the solvent density inside the sphere.

MD Simulations Setup

Using the stable ligand-OXA-48-system from previous docking and MD simulation steps, the polar residues of the system outside of the sphere boundary were neutralized and (if needed) within the middle layer as well to create a net charge of zero. This is to match the free energy contributions associated with polarization outside the sphere between the reference system of the ligand in water and the system where the ligand is in the protein (further explained in the next section).

The system was run at 298 K or 310 K, simulations were performed with the OPLS-AA force field [30] (parametrization for ligands was done with MacroModel ver. 13.3 [31]) and enveloped in a 30 Å sphere of water (TIP3P model). Nonbonded interactions up to a 10 Å cut-off were calculated explicitly, where no cut-off was used for the ligand. The time step used was 2 fs and sampling of the ligand-surrounding interaction energies was done every 25 steps. The equilibration phase for the protein-ligand simulations lasted for 2 ns with a gradual release in heavy atom restraints as the temperature increases. The subsequent data collection phase lasted for 10 ns. Corresponding simulations in the water-ligand reference system had an equilibration phase of 1 ns and a data collection phase of 1.5 ns.

The convergence of the simulations (for both protein-ligand and water-ligand systems) was estimated by comparing the differences between the two halves of the trajectories, where a difference within 2.0 kcal/mol in total potential energy was considered converged, and for the subsequent binding affinity calculations (with LIE) five converged replicates are necessary. Each simulation was run in five replicates with randomized initial velocities.

Binding Affinity Calculations with the Linear Interaction Energy (LIE) Method

The basis of the LIE method is to view when a ligand binds to a protein as the ligand transferring from one medium to another, which is its free state in water to the binding site of the protein (bound state). To determine the absolute binding free energy, both states must be considered with the ligand-ligand (intramolecular) and ligand-surrounding interactions to estimate the total difference in energy from the formation of the ligand-protein complex.

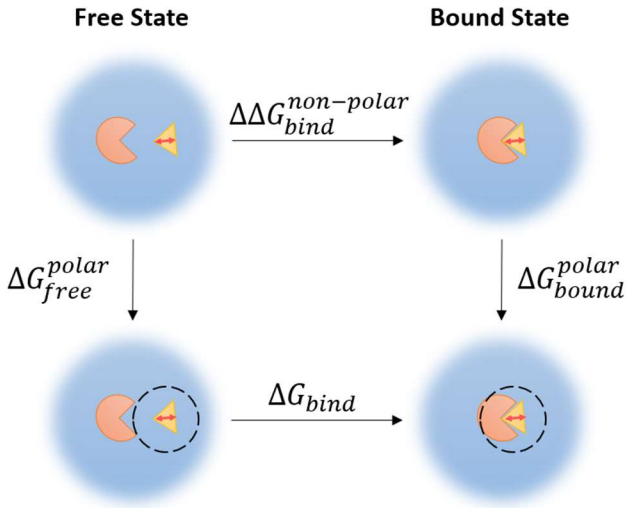

Figure 5: Thermodynamic cycle used for the LIE method in estimating the binding free energies. The orange object indicates the protein while the yellow object indicates the ligand. The dashed lines around the ligand indicate the turned-on ligand-surrounding potential energies, whereas the double-sided arrow in the ligand represents the ligand-ligand (intramolecular) potential energies.

This can be described with the thermodynamic cycle in figure 5, and from it, an expression for the binding free energies can be obtained:

$$\Delta G_{bind} = \Delta G_{bound}^{polar} - \Delta G_{free}^{polar} + \Delta\Delta G_{bind}^{non-pola} \quad (1)$$

From the equation and thermodynamic cycle, ΔG_{bound}^{polar} and ΔG_{free}^{polar} are the free energies associated with the ligand-surrounding electrostatic interaction energies with the ligand state bound in the protein and free in water, respectively. The $\Delta\Delta G_{bind}^{non-pola}$ term is the free energy difference of the ligand in bound and free state where electrostatic interactions are not considered (i.e., an unphysical, intermediate state where only the change in ligand-ligand intramolecular interactions are considered) [32]. From equation (1), the free binding energies can be expressed as the sum of the polar and non-polar components of the free energy. The LIE method attempts to estimate this via the state where only the difference in ligand-surrounding (l-s) interactions are considered – excluding the separate ligand-ligand intermediate state. This will require MD simulations of the ligand surrounded by water (free) and in the binding site (bound).

Both the water-ligand and protein-ligand simulations are run in five replicates, where for each simulation the ligand-surrounding non-polar (van der Waals, "vdW") and polar (electrostatic, "el") contributions are extracted. To estimate the total binding free energy (ΔG_{bind}^{calc}) with the LIE method, the average of the non-polar and polar potential energies ($\langle U_{l-s} \rangle$) from both ligand-surrounding systems are used in the following LIE equation:

$$\Delta G_{bind}^{calc} = \alpha\Delta\langle U_{l-s}^{vdW}\rangle + \beta\Delta\langle U_{l-s}^{el}\rangle + \gamma \quad (2)$$
$$= \alpha\left(\langle U_{l-s}^{vdW}\rangle_{protein} - \langle U_{l-s}^{vdW}\rangle_{water}\right) + \beta\left(\langle U_{l-s}^{el}\rangle_{protein} - \langle U_{l-s}^{el}\rangle_{water}\right) + \gamma$$

In this equation there are scaling factors α and β as well as the offset parameter γ. The scaling factor for non-polar interaction energies is represented by the α-term, and has been empirically

determined at the value α = 0.18 which has been proven applicable for a wide variety of ligand-receptor systems. The scaling factor for polar interaction energies is subsequently represented by the β-term, which has proven to be variable per the properties of the ligand. Two studies have been done on estimating the β-term and how to apply it in accordance to the ligand structure; Hansson et. al. [33] proposed a parametrization for uncharged ligands where the β-term varies according to the number of hydroxyl groups and charged ligands had a value of β = 0.5, whereas Almlöf et. al. [34] included values for individual functional groups where the β-term can be calculated from the standard value according to the groups included in the ligand. However, since all ligands prepared in this project carry a charge, the parametrization used by Hansson et. al. [33] was used (see table 1).

Table 1: β-parametrization proposed by Hansson et. al [33] used in this project.

Hansson et. al. [33]		
State	**OH-groups**	**β**
Charged	N/A	0.5
Neutral	0	0.43
	1	0.37
	2	0.33

Apart from the scaling factors, the offset parameter γ is considered a system-specific term that fits the scale between the experimentally determined and the calculated binding free energies, where the value has previously been found to be anywhere from γ = 18 kcal/mol to γ = -11 kcal/mol, and it appears to partly give an indication of the hydrophobicity of the binding site where a negative value indicates it is hydrophobic [35,36].

To compensate for the residues in the protein that had been neutralized (as mentioned in the previous section), as the charges may have contributed to the electrostatic interactions, an electrostatic correction term (ΔG_{corr}^{el}) was also calculated and added to the calculated binding free energy from the LIE method, see equation (3):

$$\Delta G_{corr}^{el} = 332 \sum_{p} \sum_{l} \frac{q_p \, q_l}{\varepsilon r_{pl}} \qquad (3)$$

The correction term is approximated by Coulomb's law, where q_p is the formal charge of the neutralized residue, q_l is the partial charge of the ligand atom, and r_{pl} is the distance between the ligand atom and the central atom in the neutralized residue. The dielectric constant (ε) was set to 80, which is the value for water [29].

Experimentally determined binding free energies (ΔG_{bind}^{exp}) are calculated from measurements established with *in vitro* assays, in this project from IC_{50}-values, and compared with the calculated values to estimate the affinities. This is done using the Cheng-Prusoff equation [37]:

$$\Delta G_{bind}^{exp} = -RT \ln(K_a) = RT \ln(K_d) = RT \ln(IC_{50}) + c \qquad (4)$$

The c-term in the equation is a constant specific to the assay used for determining the IC_{50}-values, where it is dependent on substrate concentration and the K_M-value. As a constant, the c-term will be included in the offset parameter γ since it will contribute to the system-specific fitting.

Results and Discussion

Structural Flexibility of OXA-48

The long flexible loop (α3-α4) would often contribute to the non-convergence of the protein in the PL-RMSD analysis, but as it has been suggested to mechanistically serve the purpose to open the binding site [19], the system was still considered to be equilibrated if this was the only big conformational change that occurred during the simulation and otherwise converged. When this has been achieved, then the system was used for further MD simulations to determine the binding free energies.

However, the protein's flexibility could affect the fit of the ligands in the binding site. The crystal structure used in this project is from OXA-48 in complex with avibactam (PDB: 4S2K), which allowed for DBO-ligands docked into the binding site to stabilize almost immediately. When the same procedure was applied for the OXA-48 apo-structure (PDB: 6P96) using avibactam as the ligand, it would rarely remain in place even if it had the same initial docking position as with the docking in the structure that had been crystallized with avibactam. From a structural analysis of the movements of the two structures without a ligand (same procedure as MD simulations for stability – 100 ns), a difference in α4 was found (see figure 6). When simulating the apo-structure the α-helix had quite large displacements over the course of the trajectory, while the structure previously in complex with avibactam had smaller displacements. The movement of α4 will affect the residues part of motif II (S118-V119-V120) in the α4-α5 loop which is part of the binding site, which in turn likely affected the stability of the ligands during the simulations. This displacement could be due to differences in the form that the structures were crystallized, it could also suggest that OXA-48 may have an induced fit mechanism or some other structural change affecting the protein dynamic. Due to time constraints this was not further investigated for the purpose of this project, as stability for a majority of the ligands was found with the crystal structure 4S2K.

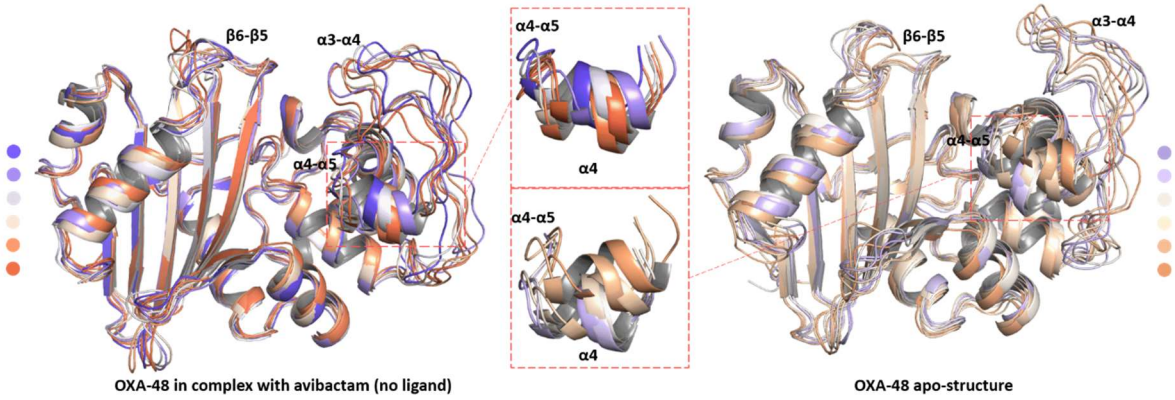

Figure 6: Frames of 100 ns MD simulations aligned on top of one another, the color gradient lilac to orange corresponds to early (lilac) to late (orange) frames (1000 in total) in the trajectories. Crystal structures pictured is OXA-48 that had been in complex with avibactam (PDB: 4S2K; left) and the apo-structure of OXA-48 (PDB: 6P96; right) with an enhanced picture of the displacement of α4 for both structures.

Carboxylation State of K73

Caution should be taken if this method is to be repeated with other inhibitors in OXA-48, as it has been applied on the basis that K73 in the binding site is neutral. It has been suggested that the mechanism of avibactam inhibition is likely not via K73 participating in its carboxylated state, so by extension, it may only be applicable for inhibitors of the DBO-scaffold. When for example analyzing the structure of a boronate-derived inhibitor covalently bound to the serine (PDB: 6V1O) [17], the lysine was carboxylated and may have played a role in the mechanism of this inhibitor. This is an area that warrants further research, as the state of K73 may be variable according to the ligand structure, apart from surrounding factors such as pH and dissolved CO_2 levels.

Molecular Docking and Ligand Positions of the Binding Site

Consistent with other studies on the mechanism of avibactam in carbapenemases [2], it was found in this project that for all the studied ligands with the DBO-scaffold, the most stable initial position from the docking in the binding site is when the carbonyl oxygen-group of the DBO-ring is positioned between the backbone hydrogens of especially Y211 and sometimes S70 (i.e., the oxyanion hole). All poses that stabilized in the subsequent MD simulations were the best scored XP poses, except for ETX-F which was a pose generated with SP, and had an initial distance to S70 of 2.3 – 2.8 Å.

During the MD simulations, having the placement of the ligand between the backbone hydrogens allowed the ligand to stay upright and in close vicinity of S70 (1.7-4.8 Å) for the mechanism (see figure 7, middle position). However, if the ligand lost the stabilizing hydrogen bonds to the backbone, for the most part, it would flip with the carbonyl oxygen toward R250 setting the ligand further away from S70 (6-8 Å; see figure 7, left position). Once the ligand is turned toward this residue during the simulation, deeper in the binding site, it remains a long distance from the reactive S70 which was deemed unproductive in terms of initiating the inhibition mechanism. On rare occasions, the ligand would also lean out of the oxyanion hole away from S70 and toward K73 and S118 as well (~5.5 Å; see figure 7, right position), where the probability of returning to the oxyanion hole is higher and the inhibition mechanism is still possible. These positions are represented in the histograms of each ligand. The big distance intervals corresponding to the ligand staying between the backbone hydrogens (1.7-4.8 Å) is due to whether the S70 hydroxyl group is turned towards or away from the ligand during the simulations. When turned away, the S70 faced K73 which considering the mechanism (see figure 2) would be part of the K73-mediated deprotonation.

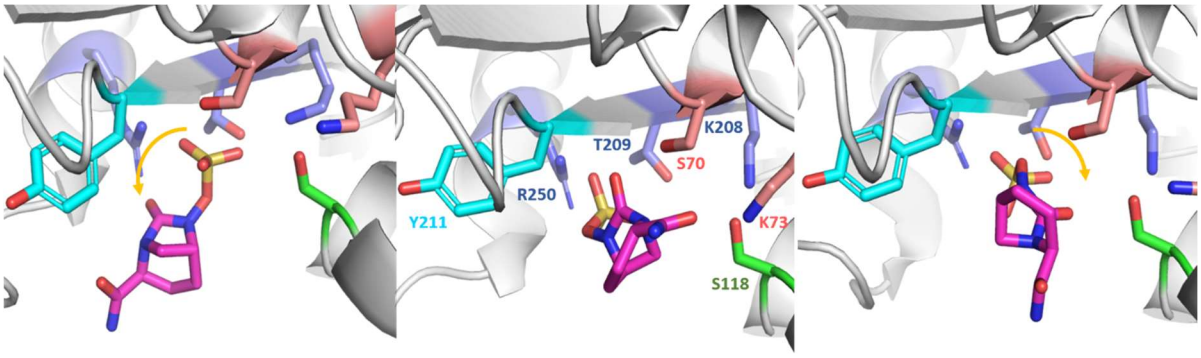

Figure 7: The positions of the ligands with the DBO-scaffold (in picture avibactam) in the binding site of OXA-48 during the MD simulations. The middle picture depicts the ligand in the oxyanion hole, the left picture depicts the ligand position towards R250 and the right picture depicts the ligand position towards K73/S118.

Avibactam

The varied effect of avibactam as an inhibitor of OXA-48 becomes clearer when the distribution of its positions within the binding site is considered (also shown in figure 7). While it has a slightly higher probability to remain in the oxyanion hole (~4.7 Å with S70 turned away), the tendency to flip towards R250 is almost just as likely to happen (~6.57 Å) as shown in figure 8. The standard deviation from the electrostatic potential energies in the protein is also indicative of this (see table 2), as the position of the ligand in the binding site affects the interactions.

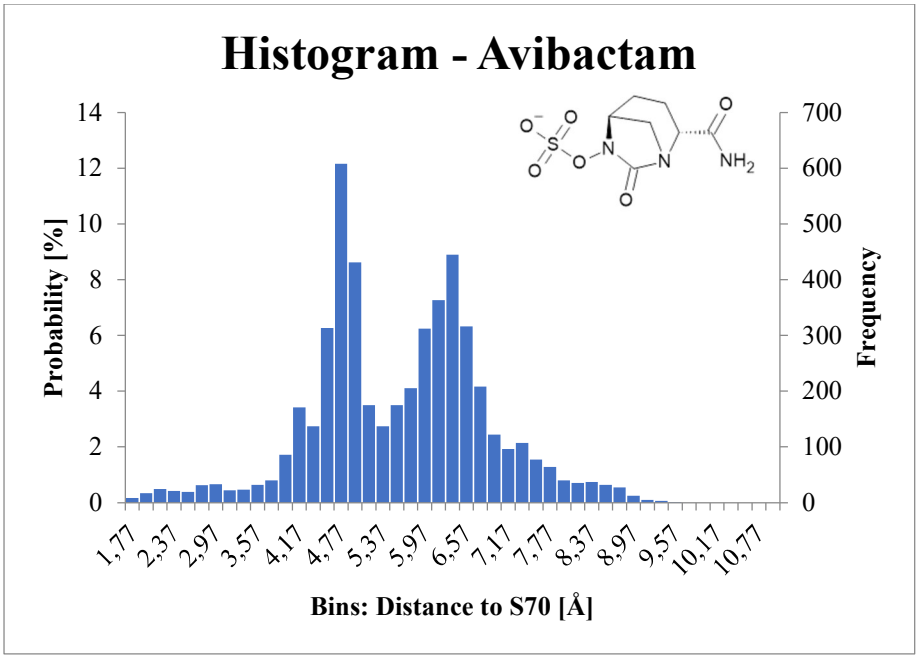

Figure 8: Histogram of avibactam positions in relation to the distance measured from the carbonyl oxygen of the DBO-ring to the hydroxyl of S70. Histogram compounded of distances measured from five replicate simulations run for 50 ns.

Relebactam

In pH 7.0, relebactam exists as a zwitterion and has a flexible structure with the two chains from the DBO-ring. This makes this ligand a special case, as discussed by Almlöf et. al. [34], because the opposite charges do not make the ligand behave like it is neutral, and separate scaling factors than those used in this project may be necessary – which, at this time, have not been resolved. When analyzing simulations of the ligand surrounded by only water, the flexible chains of the ligand tended to try to pull the opposite charged functional groups toward each other but got no closer than 6 Å due to the rigidity of the DBO-ring (see figure 9). This conformational change, beyond the need for different scaling factors, affected the electrostatic interactions for the reference system in water as well.

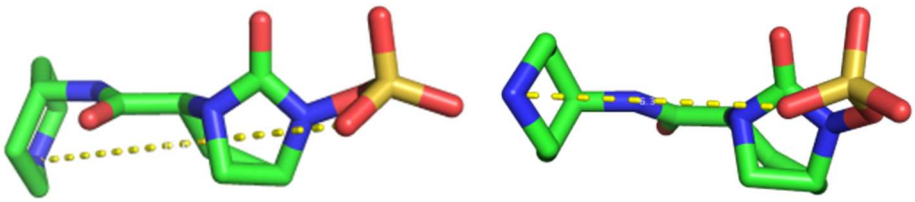

Figure 9: Relebactam's alternating conformations found during the water simulations. The outstretched (left) conformation with a distance between the opposite charges in the cationic piperidine ring and the anionic sulphate group at 10.8 Å, as well as cradled (right) conformation with a distance between the opposite charges at 6.3 Å.

Beyond the simulations in water, the ligand rarely stays between the backbone hydrogens in the protein. It is more inclined to turn towards R250 compared to avibactam (see figure 10), which similarly to avibactam majorly affected its electrostatic potential energies as they rarely converged. Comparatively, relebactam is also a bigger ligand than the rest of the ligands, and as the binding site of OXA-48 is rather shallow the size difference could contribute to its instability by being partly exposed to surrounding water (especially the piperidne ring).

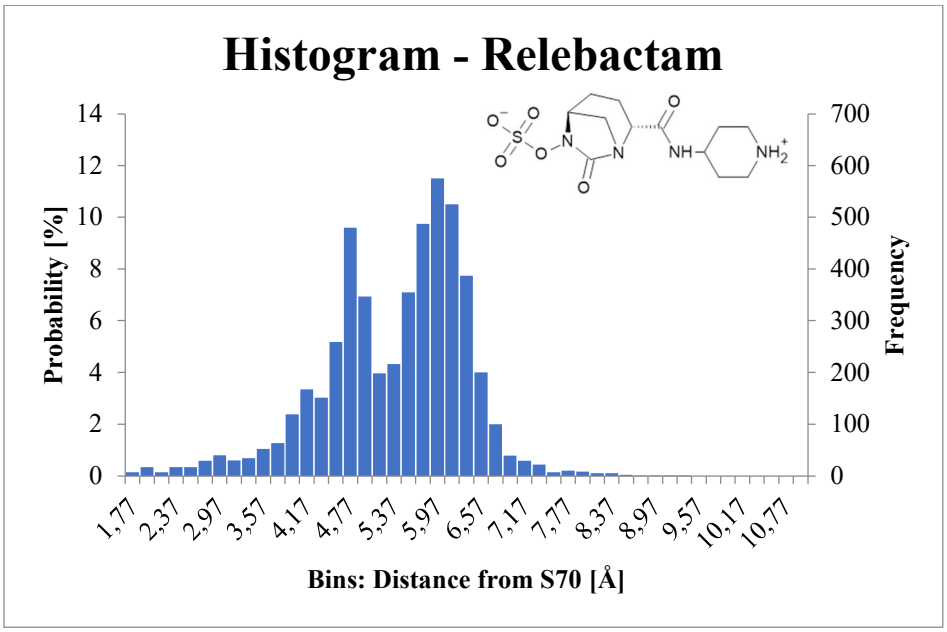

Figure 10: Histogram of relebactams positions in relation to the distance measured from the carbonyl oxygen of the DBO-ring to the hydroxyl of S70. Histogram compounded of distances measured from five replicate simulations run for 50 ns.

The very low electrostatic potential energies in the protein are partly due to the ability to form salt bridges from both of the charged groups. Similar to avibactam, the sulfate group can form salt bridges to both the positively charged R250 and K208 (where it is more inclined toward R250), however, the positive charge of the ligand also allows for a salt bridge to form with the negatively charged D101, which is part of the flexible α3-α4 loop. The electrostatic potential energy of the ligand in the protein is drastically different depending on whether this salt bridge to the α3-α4 loop occurs or not, which is reflected in the standard deviation of $\langle U_{l-s}^{el} \rangle_{protein}$ (see table 2).

ETX and ETX-F

ETX was one of the more stable ligands with regards to staying between the backbone hydrogens. In figure 11 this is mainly represented in the peak around 2.97 Å. Another interesting point is, unlike simulations with relebactam and avibactam, for a majority of the simulations the S70 hydroxyl was turned towards ETX and would interact with the ligand. This is likely due to ETX from the MD simulations being positioned a bit higher up in the oxyanion hole compared to relebactam and avibactam, bringing it closer to the backbone hydrogen of S70 – which allowed for more consistent interactions with the catalytic residue. On occasion, the ligand could lose the interactions with the backbone as well and flip in the binding site.

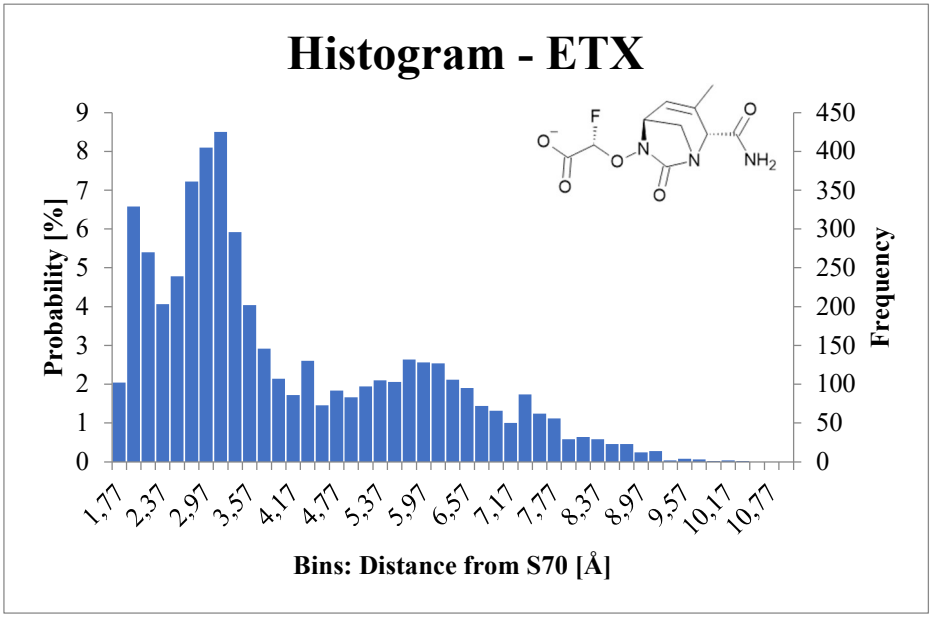

Figure 11: Histogram of ETX positions in relation to the distance measured from the carbonyl oxygen of the DBO-ring to the hydroxyl of S70. Histogram compounded of distances measured from five replicate simulations run for 50 ns.

ETX did not converge its electrostatic potential energies from the water runs. To investigate why this may have been the case, the fluorine atom was replaced with a hydrogen to see if it affected the values (i.e., the ETX-F ligand was investigated). In water simulations for ETX-F the electrostatic potential energies converged. From the trajectories, there appeared to be no tangible difference in the way the ligands interacted with the solvent and both were within the spherical boundary. This solidified the idea that the fluorine-atom may have been the source of error for ETX.

From plotting the electrostatic potential energies from the water runs of ETX, there appear to be two energy levels present (see appendix A). From these two energy levels, the average structure was constructed via the Q-prep function, and there's a possibility that the fluorine-atom in the structure has intramolecular interactions when it has more freedom of movement in the water, creating a conformational change which results in the electrostatic potential energy fluctuating (see figure 12). The non-convergence of ETX in water could be due to the time used for the water-ligand simulations. The set data collection phase for the water-ligand simulations is much shorter than the data collection phase used for the protein-ligand simulations, and fluctuations in a smaller dataset will reflect in the convergence. The general workflow applied from the work of Shamsudin et. al. [16] considered more rigid ligands, where in their free state in water such conformational changes were unlikely to occur thus the simulations could afford to be shorter.

In future work, the data collection phase in water for flexible ligands should be extended. But for the setup used in this method, what could be done is to apply MD simulations similar to the ones used to determine model stability. By measuring the distances shown in figure 12 throughout the simulations, a distribution can be made and from the occurrence of the two conformations it can be determined whether the intramolecular interactions would affect the convergence from a longer trajectory. Due to time constraints, however, this was not done in this work.

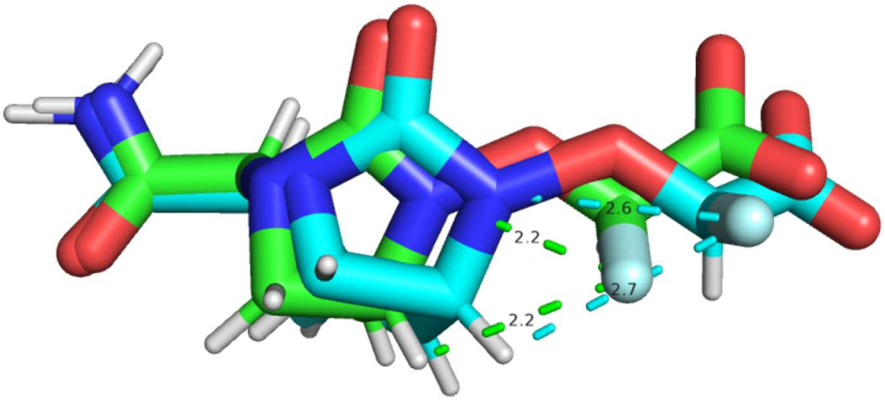

Figure 12: Alignment of the average structures of the two energy levels of ETX with measured distances between the fluorine-atom and N6 as well as the fluorine-atom and the C5 hydrogen. The structure represents the lower electrostatic potential energy in green and the structure represents the higher electrostatic potential energy in cyan.

In the case of ETX-F, it was very stable in its initial docking position between the backbone hydrogens (figure 13). Similarly, with the binding free energy simulations of the ligand, the potential energy values had minimal deviations – even during the water simulations, as opposed to ETX (see table 2).

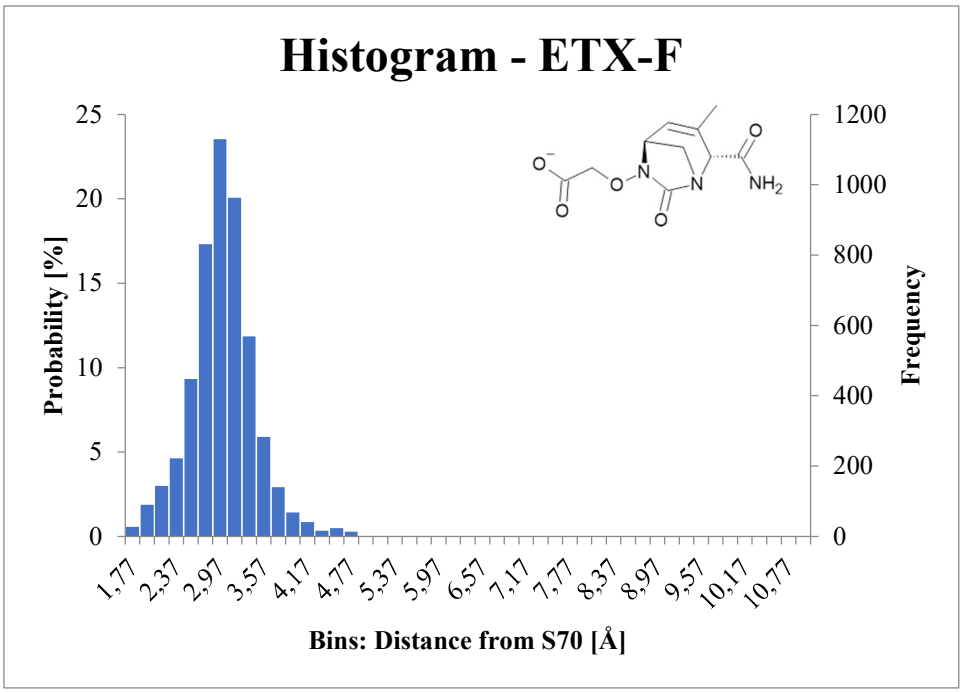

Figure 13: Histogram of ETX-F positions in relation to the distance measured from the carbonyl oxygen of the DBO-ring to the hydroxyl of S70. Histogram compounded of distances measured from five replicate simulations run for 50 ns.

For both ETX and ETX-F, the addition of a methyl group on that C3 in the DBO-ring favored hydrophobic interactions with a hydrophobic pocket made up of residues on the β5-β6 loop. Had the methyl group been put on the other side of the endocyclic double bond (i.e., C4), the methyl group would instead be exposed to solvent (see appendix B), and from MD simulations the stability of this ligand could not be achieved (see appendix C). This observation could also be connected to the lower IC_{50} value of ETX (methyl group on C3) at 0.015 µM, whereas the similar structure with the methyl-group on C4 had an IC_{50} of 0.070 µM against OXA-48 [14].

An interesting part of the structure that also appeared to play a role in its stability in the binding site is that the chain with the carboxylic acid is one atom longer than the ligands with the sulfate group as the anionic group. This ensured that the amide group on the opposite side of the ligand could more consistently interact with R214 and various backbone carboxyl-groups in the β5-β6 loop. As discussed by King et. al. [2], the β5-β6 loop is important for the stabilization of the amide group in the case of avibactam and a point of interest for future drug design. Due to the elongation of the anionic chain, this stabilization appears to be achieved, while still maintaining the other interactions deemed to stabilize the ligand i.e., the salt bridge to the basic patch and the interactions with the backbone hydrogens.

In order to compare ETX and ETX-F to a ligand that had a different anionic group, the ligand durlobactam was also briefly studied but not to the full extent of the method. Like avibactam, durlobactam's anionic group is a sulfate group, but is set apart by the addition of the stabilizing methyl group and the endocyclic double bond. For this ligand, however, stability in the binding site could not be achieved (see appendix D). The initial docking pose was the same as with all other ligands, but it would not remain between the backbone hydrogens during simulations and would take on various positions in the binding site. For this ligand, more poses from the docking needs to be evaluated as well as more simulations to explore the behavior of this ligand in OXA-48 – both MD simulations for stability and binding free energy determination.

Binding Free Energy Determination

The resulting binding free energies for each ligand have been summarized in table 2 where the electrostatic correction term of -0.35 kcal/mol (see appendix E) was applied and is represented in the values of table 2. The standard deviations of the potential energies (both from the water and protein simulations) are the deviations between the values from the five converged simulations used for the average. The standard deviations in the calculated binding free energies are the pooled standard deviations from these potential energies. As already mentioned, relebactam and ETX turned into special cases, thus the standard deviation for the electrostatic potential energies for the protein and the water runs respectively are high.

Table 2: Summary of the total average of potential energies for the water and protein runs with standard deviations. The binding free energies are reported in kcal/mol with standard deviations, and the corresponding experimental binding free energies are calculated from the IC_{50}-values of the ligands listed in figure 1 using equation 4.

Inhibitor	$\langle U_{l-s}^{vdW} \rangle_{water}$	$\langle U_{l-s}^{el} \rangle_{water}$	$\langle U_{l-s}^{vdW} \rangle_{protein}$	$\langle U_{l-s}^{el} \rangle_{protein}$	ΔG_{bind}^{calc}	ΔG_{bind}^{exp}
Avibactam	-10.51 ± 0.03	-179.61 ± 0.50	-21.19 ± 0.85	-158.21 ± 1.52	8.78 ± 1.23	-9.56
Relebactam	-14.93 ± 0.02	-262.70 ± 0.88	-28.97 ± 1.72	-281.00 ± 4.17	-11.67 ± 3.19	-5.74
ETX	-8.61 ± 0.05	-217.18 ± 1.51	-22.61 ± 1.01	-183.83 ± 0.51	14.15 ± 0.80	-10.66
ETX-F	-9.20 ± 0.05	-208.23 ± 0.49	-23.72 ± 0.43	-183.45 ± 0.68	9.78 ± 0.56	-9.94

A general value of the system for the offset parameter γ could not be determined as it would require three different ligands where the potential energies had converged. However, for the two ligands that achieved convergence – avibactam and ETX-F – the γ value could be determined separately from the difference of the calculated and experimental ΔG_{bind} as -18.34 kcal/mol and -19.71 kcal/mol respectively, which are within 2 kcal/mol of one another. Whereas for relebactam the γ would be 5.94 kcal/mol and for ETX -24.82 kcal/mol. To more accurately attempt to determine the system-specific γ, more ligands would need to be studied. However,

the implications of the value of γ being out of scope to previous studies may be that the flexibility of OXA-48 adds to the value, as differences in entropy also contributes to the offset parameter.

As the ΔG_{bind}^{calc} of relebactam cannot be accurately determined due to β = 0.5 not corresponding to its flexible, zwitterionic nature, an attempt to estimate the β-term was done using the mean of the two γ-values of avibactam and ETX-F and by rearranging equation 2. The results gave β = 1.54 from the potential energies achieved for relebactam in this work.

From the binding free energies, the poor overlap between the calculated values and the experimental values could be due to the Michaelis Complex not being as important as the reaction rate of the mechanism. In other words, the formation of the covalent bond between S70 and the ligand may happen so quickly that the stability of the ligand in the binding site may not have as much bearing on the activity, and the subsequent measurements of activity from other studies. However, for the future design of an inhibitor, it may still be worthwhile to investigate a molecular structure that can stay stable in OXA-48 as well as have a high reaction rate.

Conclusions

The significance of this work is that it can be a puzzle piece to a bigger issue pertaining to the drug design of β-lactamase inhibitors, especially to find a lead with good stability in the binding site of OXA-48. From the resulting binding affinities found in this work, the protein appears to be a relatively poor binder, and it can be surmised that the initial interactions of the Michaelis Complex may not weigh as heavily as the reaction rate of the covalent bond formation. However, the initial stability in the binding site can be improved with the addition of a methyl group at the C3 carbon as it provided hydrophobic interactions with the protein, and through the elongation of the chain with the anionic group there were more consistent interactions with residues such as R214 in the β5-β6 loop by the amide in C2. It has also been confirmed that the initial docking position in the oxyanion hole is generally favored for ligands of the DBO-scaffold. This project also elucidates the applicability of structure-based virtual screening methods to gain a better understanding of the behavior of drug molecules in its target protein.

However, the complexity of OXA-48 warrants further research, as a greater understanding of the protein itself is needed to corroborate these findings. For example, when the carboxylation of K73 is relevant; is it mainly for the degradation of antibiotics, or does it also play a role in the inhibition mechanism of some β-lactamase inhibitors? Also, investigations should be done on how the flexibility of the protein may affect the binding of substrates, and if OXA-48 truly has an induced fit mechanism or something otherwise affecting the protein dynamic.

Beyond the structural research of the protein, further investigation should be done with more ligands of different scaffolds to either confirm or deny whether the stability of the ligand in the binding site or the catalytic rate is what contributes more heavily to the experimentally determined kinetic parameters of the ligands. By gaining a better understanding on the basis of the inhibition mechanism, the development of inhibitors can become more focused. More simulation work can also be done for ligands in OXA-48 in order to establish a system specific γ-value for binding affinity estimations using LIE, where results in this work could indicate that the offset parameter can be at a value around γ ≈ -19 kcal/mol for flexible ligand-protein systems.

Acknowledgment

I would like to thank my supervisor Yasmin Binti Shamsudin for your wonderful guidance, thank you for teaching me many new things and for motivating me. Thank you for the time you have given and for your patience in this project.

I would also like to thank my research group, Isabell Lindahl and Alexander Lidén, for being supportive and encouraging throughout this work.

References

[1] Murray, C. J., Ikuta, K. S., Sharara, F., Swetschinski, L., Aguilar, G. R., Gray, A., Han, C., Bisignano, C., Rao, P., Wool, E., Johnson, S. C., Browne, A. J., Chipeta, M. G., Fell, F., Hackett, S., Haines-Woodhouse, G., Hamadani, B. H. K., Kumaran, E. A. P., McManigal, B., Agarwal, R., Akech, S., Albertson, S., Amuasi, J., Andrews, J., Aravkin, A., Ashley, E., Bailey, F., Baker, S., Basnyat, B., Bekker, A., Bender, R., Bethou, A., Bielicki, J., Boonkasidecha, S., Bukosia, J., Carvalheiro, C., Castañeda-Orjuela, C., Chansamouth, V., Chaurasia, S., Chiurchiù, S., Chowdhury, F., Cook, A. J., Cooper, B., Cressey, T. R., Criollo-Mora, E., Cunningham, M., Darboe, S., Day, N. P. J., Luca, M. D., Dokova, K., Dramowski, A., Dunachie, S. J., Eckmanns, T., Eibach, D., Emami, A., Feasey, N., Fisher-Pearson, N., Forrest, K., Garrett, D., Gastmeier, P., Giref, A. Z., Greer, R. C., Gupta, V., Haller, S., Haselbeck, A., Hay, S. I., Holm, M., Hopkins, S., Iregbu, K. C., Jacobs, J., Jarovsky, D., Javanmardi, F., Khorana, M., Kissoon, N., Kobeissi, E., Kostyanev, T., Krapp, F., Krumkamp, R., Kumar, A., Kyu, H. H., Lim, C., Limmathurotsakul, D., Loftus, M. J., Lunn, M., Ma, J., Mturi, N., Munera-Huertas, T., Musicha, P., Mussi-Pinhata, M. M., Nakamura, T., Nanavati, R., Nangia, S., Newton, P., Ngoun, C., Novotney, A., Nwakanma, D., Obiero, C. W., Olivas-Martinez, A., Olliaro, P., Ooko, E., Ortiz-Brizuela, E., Peleg, A. Y., Perrone, C., Plakkal, N., Ponce-de-Leon, A., Raad, M., Ramdin, T., Riddell, A., Roberts, T., Robotham, J. V., Roca, A., Rudd, K. E., Russell, N., Schnall, J., Scott, J. A. G., Shivamallappa, M., Sifuentes-Osornio, J., Steenkeste, N., Stewardson, A. J., Stoeva, T., Tasak, N., Thaiprakong, A., Thwaites, G., Turner, C., Turner, P., Doorn, H. R. van, Velaphi, S., Vongpradith, A., Vu, H., Walsh, T., Waner, S., Wangrangsimakul, T., Wozniak, T., Zheng, P., Sartorius, B., Lopez, A. D., Stergachis, A., Moore, C., Dolecek, C., Naghavi, M. *The Lancet* 2022, *399*, 629–655.

[2] King, D. T., King, A. M., Lal, S. M., Wright, G. D., Strynadka, N. C. J. *ACS Infect. Dis.* 2015, *1*, 175–184.

[3] Bush, K., Jacoby, G. A. *Antimicrob Agents Chemother* 2010, *54*, 969–976.

[4] Yoon, E.-J., Jeong, S. H. *Journal of Antimicrobial Chemotherapy* 2021, *76*, 836–864.

[5] Evans, B. A., Amyes, S. G. B. *Clin Microbiol Rev* 2014, *27*, 241–263.

[6] Silver, L. L. *Clin Microbiol Rev* 2011, *24*, 71–109.

[7] Tooke, C. L., Hinchliffe, P., Bragginton, E. C., Colenso, C. K., Hirvonen, V. H. A., Takebayashi, Y., Spencer, J. *J Mol Biol* 2019, *431*, 3472–3500.

[8] Totir, M. A., Cha, J., Ishiwata, A., Wang, B., Sheri, A., Anderson, V. E., Buynak, J., Mobashery, S., Carey, P. R. *Biochemistry* 2008, *47*, 4094–4101.

[9] Leonard, D. A., Bonomo, R. A., Powers, R. A. *Acc Chem Res* 2013, *46*, 2407–2415.

[10] Coleman, K. *Current Opinion in Microbiology* 2011, *14*, 550–555.

[11] Zasowski, E. J., Rybak, J. M., Rybak, M. J. *Pharmacotherapy* 2015, *35*, 755–770.

[12] Ehmann, D. E., Jahić, H., Ross, P. L., Gu, R.-F., Hu, J., Durand-Réville, T. F., Lahiri, S., Thresher, J., Livchak, S., Gao, N., Palmer, T., Walkup, G. K., Fisher, S. L. *J Biol Chem* 2013, *288*, 27960–27971.

[13] Vázquez-Ucha, J. C., Arca-Suárez, J., Bou, G., Beceiro, A. *Int J Mol Sci* 2020, *21*, E9308.

[14] Durand-Réville, T. F., Comita-Prevoir, J., Zhang, J., Wu, X., May-Dracka, T. L., Romero, J. A. C., Wu, F., Chen, A., Shapiro, A. B., Carter, N. M., McLeod, S. M., Giacobbe, R. A., Verheijen, J. C., Lahiri, S. D., Sacco, M. D., Chen, Y., O'Donnell, J. P., Miller, A. A., Mueller, J. P., Tommasi, R. A. *J Med Chem* 2020, *63*, 12511–12525.

[15] Maia, E. H. B., Assis, L. C., de Oliveira, T. A., da Silva, A. M., Taranto, A. G. *Frontiers in Chemistry* 2020, *8*.

[16] Shamsudin Khan, Y., Gutiérrez-de-Terán, H., Boukharta, L., Åqvist, J. *J. Chem. Inf. Model.* 2014, *54*, 1488–1499.
[17] Lomovskaya, O., Tsivkovski, R., Sun, D., Reddy, R., Totrov, M., Hecker, S., Griffith, D., Loutit, J., Dudley, M. *Front Microbiol* 2021, *12*, 697180.
[18] Docquier, J.-D., Calderone, V., De Luca, F., Benvenuti, M., Giuliani, F., Bellucci, L., Tafi, A., Nordmann, P., Botta, M., Rossolini, G. M., Mangani, S. *Chemistry & Biology* 2009, *16*, 540–547.
[19] Smith, C. A., Stewart, N. K., Toth, M., Vakulenko, S. B. *Antimicrobial Agents and Chemotherapy* 2019, *63*, e01202-19.
[20] Chiou, J., Cheng, Q., Shum, P. T.-F., Wong, M. H.-Y., Chan, E. W.-C., Chen, S. *Int J Mol Sci* 2021, *22*, 11480.
[21] van Groesen, E., Lohans, C. T., Brem, J., Aertker, K. M. J., Claridge, T. D. W., Schofield, C. J. *Chemistry – A European Journal* 2019, *25*, 11837–11841.
[22] Madhavi Sastry, G., Adzhigirey, M., Day, T., Annabhimoju, R., Sherman, W. *J Comput Aided Mol Des* 2013, *27*, 221–234.
[23] *Maestro, version 13.0*, Schrödinger, LLC: New York, 2021.
[24] Lu, C., Wu, C., Ghoreishi, D., Chen, W., Wang, L., Damm, W., Ross, G. A., Dahlgren, M. K., Russell, E., Von Bargen, C. D., Abel, R., Friesner, R. A., Harder, E. D. *J. Chem. Theory Comput.* 2021, *17*, 4291–4300.
[25] *LigPrep*, Schrödinger, LLC: New York, 2021.
[26] *GLIDE, version 9.3*, Schrödinger, LLC: New York, 2021.
[27] *Desmond Molecular Dynamics System, version 6.8*, D. E. Shaw Research, New York. Maestro-Desmond Interoperability Tools, Schrödinger, New York, 2021.
[28] Jorgensen, W. L., Chandrasekhar, J., Madura, J. D., Impey, R. W., Klein, M. L. *J. Chem. Phys.* 1983, *79*, 926–935.
[29] Marelius, J., Kolmodin, K., Feierberg, I., Åqvist, J. *J Mol Graph Model* 1998, *16*, 213–225, 261.
[30] Jorgensen, W. L., Maxwell, D. S., Tirado-Rives, J. *J. Am. Chem. Soc.* 1996, *118*, 11225–11236.
[31] *MacroModel, version 13.3*, Schrödinger, LLC: New York, 2021.
[32] Gutiérrez-de-Terán, H., Aqvist, J. *Methods Mol Biol* 2012, *819*, 305–323.
[33] Hansson, T., Marelius, J., Åqvist, J. *J Comput Aided Mol Des* 1998, *12*, 27–35.
[34] Almlöf, M., Carlsson, J., Åqvist, J. *J Chem Theory Comput* 2007, *3*, 2162–2175.
[35] Carlsson, J., Boukharta, L., Åqvist, J. *J. Med. Chem.* 2008, *51*, 2648–2656.
[36] Mishra, S. K., Sund, J., Åqvist, J., Koča, J. *J Comput Chem* 2012, *33*, 2340–2350.
[37] Yung-Chi, C., Prusoff, W. H. *Biochemical Pharmacology* 1973, *22*, 3099–3108.

Appendix

A. ETX: Electrostatic Potential Energies of the Two Conformations

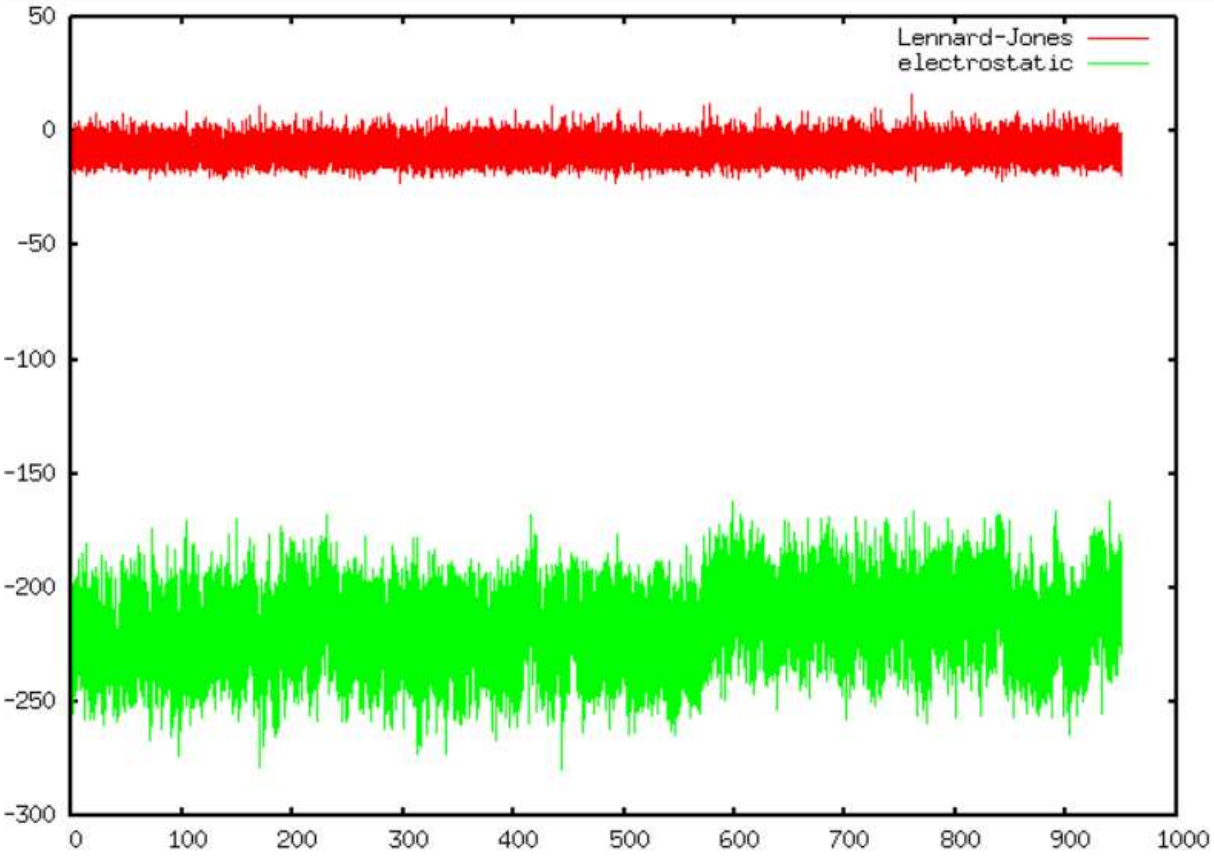

Figure 14: Plot of the Lennard-Jones (van der Waals, red) and electrostatic (green) potential energies during the reference water simulations with ETX. Two energetic levels can be seen between frames 0-550 and 550-950 for the electrostatic potential energies corresponding to two potential conformations of the ligand.

B. ETX' – structure with a methyl group at C4

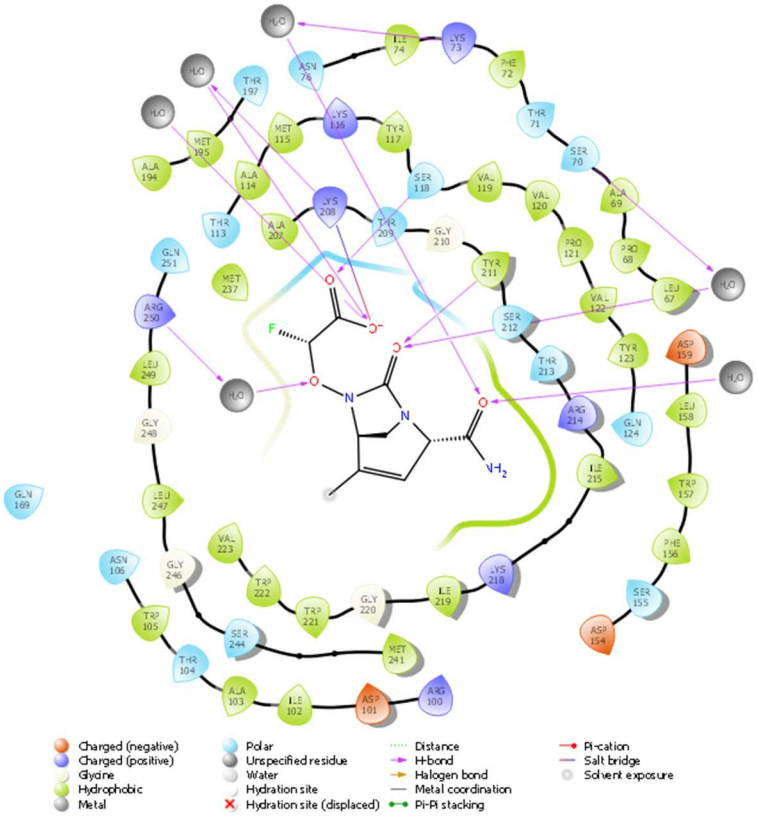

Figure 15: Ligand interaction map of a similar structure to ETX (aka ETX') but with the methyl group at C4 where it is exposed to solvent.

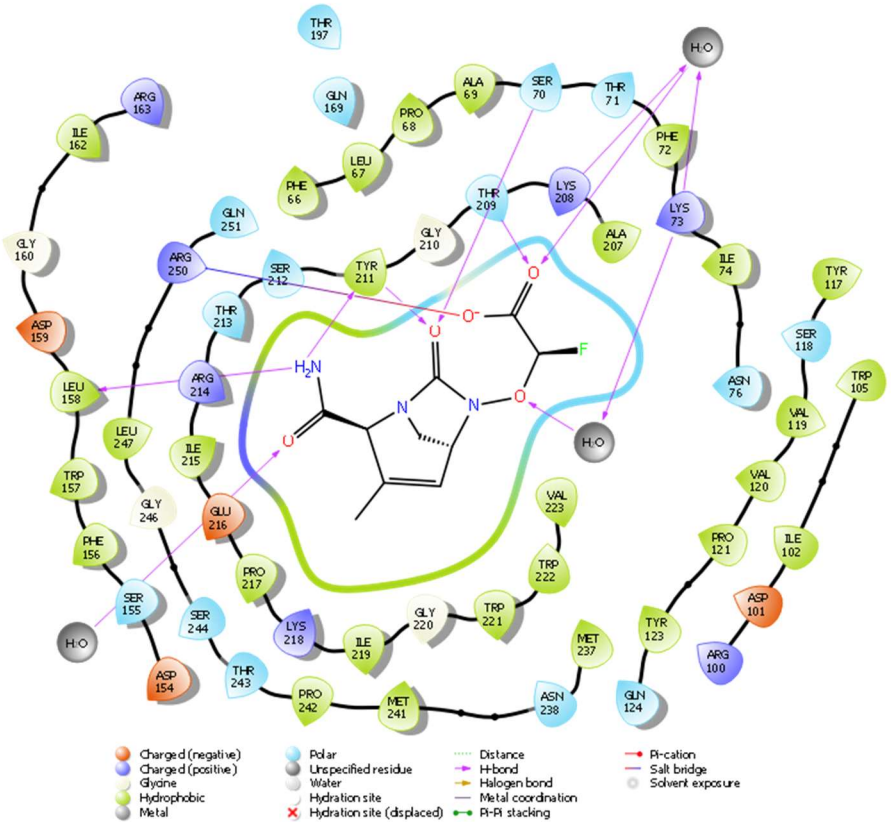

Figure 16: Ligand interaction map of ETX, where the methyl group is towards a hydrophobic pocket.

C. ETX': Distribution of Positions

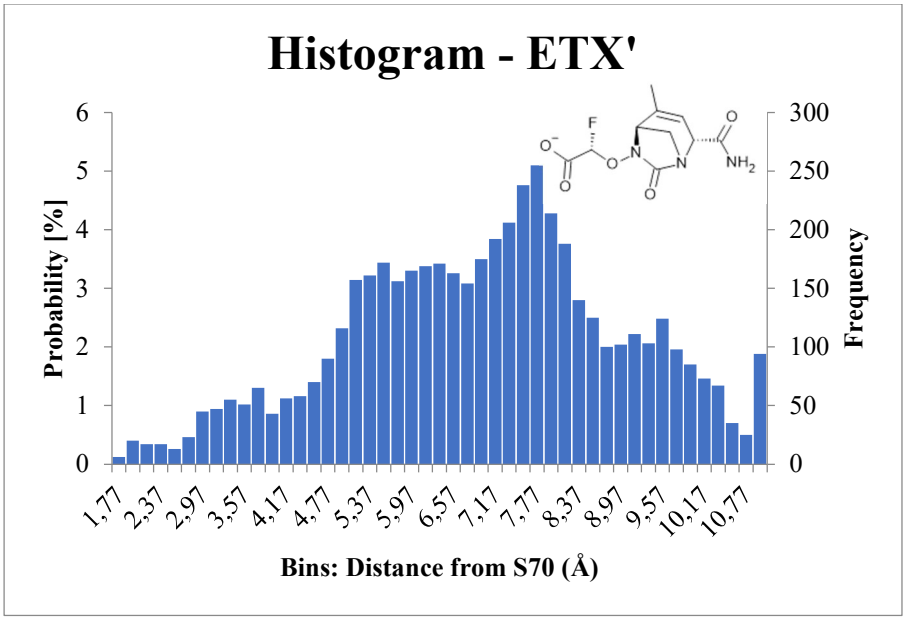

Figure 17: Histogram of ETX' positions in relation to the distance measured from the carbonyl oxygen of the DBO-ring to the hydroxyl of S70. Histogram with the combined distances measured from five replicate simulations run for 50 ns.

D. Durlobactam: Distribution of Positions

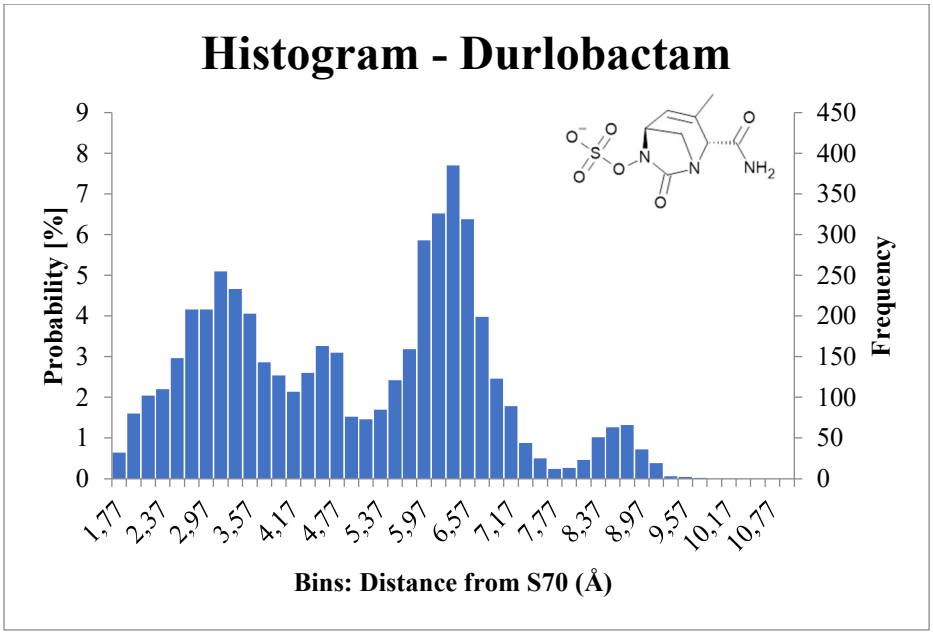

Figure 18: Histogram of durlobactam positions in relation to the distance measured from the carbonyl oxygen of the DBO-ring to the hydroxyl of S70. Histogram with the combined distances measured from five replicate simulations run for 50 ns.

E. Electrostatic Correction Term

Residues neutralized within the 30 Å sphere; D82 and D230. Residues neutralized outside the 30 Å sphere: K51, not included in determining the correction term. K73 was neutralized based on the inhibition mechanism. The average electrostatic potential energy between the ligand and each neutralized residue was sampled from five separate simulations. The electrostatic correction term applied in the final calculations was the one without the K73 contribution to stay aligned with the basis of the method, however, K73 has a varied contribution when applied.

Table 3: Average electrostatic contributions of each neutralized residue to determine the ΔG_{corr}^{el}, where the values are represented in kcal/mol.

ΔG_{corr}^{el} (kcal/mol)	Sim. 1	Sim. 2	Sim. 3	Sim. 4	Sim. 5	Total average
w/ K73 contribution	-0,88	-1,35	-3,29	-1,79	-3,90	-2,24 ± 1,16
w/o K73 contribution	-0,49	-0,49	-0,25	-0,29	-0,24	-0,35 ± 0,11